High Range Resolution at Reduced Sampling Rates in OFDM Systems Exploiting Pilot Aliasing

Abdelali Arous, *Graduate Student Member, IEEE*, Salah Eddine Zegrar, *Graduate Student Member, IEEE*, and Hüseyin Arslan, *Fellow, IEEE*

***Abstract*—High range resolution (HRR) is critical for automotive radar where it is directly dependent on the available transmission bandwidth. However, HRR sensing for OFDM entails high sampling frequencies, which extends the system's complexity and requires costly receivers. In this letter, we present an approach for achieving HRR with a reduced sampling rate by exploiting pilots aliasing in OFDM systems. In particular, the pilots take a ladder shape in the time-frequency lattice such that under-sampling the received signal causes aliasing in the pilot symbols with zero-interference from the data. The proposed approach allows low-cost sensors to obtain the sensing information without losing the range-velocity resolution.**

***Index Terms*—OFDM, sub-Nyquist sampling, high range resolution, JSAC, aliasing.**

I. Introduction

SIXTH generation (6G) envisages ubiquitous connectivity not only for communication but also other purposes such as sensing [1]. Applications as autonomous driving present scenarios where both applications are simultaneously required, leading to the popularization of joint sensing and communication (JSAC) paradigm [2]. Given that orthogonal frequency division multiplexing (OFDM) is the most popular communication technique, a significant amount of JSAC work tries to integrate sensing functionality in OFDM systems [3], [4]. One of the major challenges in this regard is to ensure reliable communication while providing high sensing resolution. The range resolution is contingent upon the extent of radio-frequency (RF) bandwidth that is accessible, with broader bandwidth producing higher resolution. Sampling a wide bandwidth requires high-speed analog-to-digital converters (ADCs) and digital-to-analog converters (DACs) to construct the signal at the receiver and transmitter sides for OFDM systems [5]. However, the utilization of these costly and energy-intensive apparatuses is unattainable for low-cost sensors. Moreover, deploying multiple sensors in self-driving cars necessitates the integration of numerous ADCs and DACs, which results in increased costs and power consumption. Therefore, studies in [6], [7], [8], [9] explore low sampling rate techniques for OFDM radar while retaining the HRR and data communication.

Manuscript received 12 September 2023; revised 15 January 2024; accepted 4 February 2024. Date of publication 7 February 2024; date of current version 11 April 2024. This work was supported by the Scientific and Technological Research Council of Turkey (TUBITAK) under Grant 123E514. The associate editor coordinating the review of this article and approving it for publication was Q. Wu. *(Corresponding author: Abdelali Arous.)*

The authors are with the Department of Electrical and Electronics Engineering, Istanbul Medipol University, 34810 Istanbul, Turkey (e-mail: abdelali.arous@std.medipol.edu.tr; salah.zegrar@std.medipol.edu.tr; huseyinarslan@medipol.edu.tr).

Digital Object Identifier 10.1109/LWC.2024.3363449

Stepped-carrier OFDM (SC-OFDM) [6] divides symbols into group of sub-symbols, with each sub-symbol being transmitted using a particular carrier frequency until the entire bandwidth is fully covered. This way the HRR is achieved with lower sampling rates for both DAC and ADC, at the expense of a lower maximal unambiguous velocity and a fast-settling time of the phase locked loop for synchronization. Similarly, [7] incorporates a random non-equidistant frequency hopping pattern using narrowband OFDM to preserve the maximum ambiguities with low sampling rate utilizing compressed sensing. Nevertheless, it adds more computational complexity overhead to the radar system. The work described in [8] uses a frequency comb composed of multiple carrier frequencies at both ends to upconvert and downconvert the signal, generating identical OFDM signals in different subbands spanning the desired RF bandwidth. However, it elevates hardware complexity and power consumption, along with perfect synchronization requirements. Another technique is proposed in [9], referred to as subcarrier aliasing OFDM (SA-OFDM), which leaves empty subcarriers between data subcarriers in each symbol. Thus after under-sampling, the aliased subcarriers will slip into those empty subcarriers. Thus, a low ADC sampling rate according to the under-sampling factor is achieved, at the expense of downgraded maximum unambiguous range. Finally, the work in [10] improves communication-assisted sensing performance by exploiting pilot sequences used for channel estimation.

Motivated by the aforementioned concerns, in this letter, we propose an OFDM transceiver design to obtain HRR sensing with a sub-Nyquist sampling rate for low-end low-complex devices. First, we analytically show that the effect of under-sampling the received OFDM signal under doubly dispersive channels causes aliasing between the subcarriers in the frequency domain. Building on these results, a pilot structure is adopted such that after under-sampling the received OFDM signal, pilot symbols are aliased with each other free of interference from data subcarriers. Also, These pilots are distributed in the time-frequency lattice such that the range-Doppler map (RDM) is reconstructed with reduced computations, ADC speeds, and with HRR detection capabilities. The complexity of the proposed technique is considerably less than that of the state of-the-art techniques while achieving comparable performance and conserving data communication performance. Nonetheless, as the under-sampling ratio increases, the unambiguous range decrease while the aliasing effect becomes more prominent, resulting in a higher signal-to-noise ratio (SNR) loss for the aliased subcarriers.[1]

[1]*Notation*: We use capital letters to signify column vectors and boldface ones for matrices. $[\alpha]_\beta$ is The modulo β of α. The convolution operator, the Big O notation and the logarithmic base 2 are denoted by $(*)$, $\mathcal{O}$ and $\log_2$, respectively. $\delta(.)$, $\mathbb{Q}$ and $\Re$ are the Dirac-delta function, set of rational numbers and the real part of a signal, respectively.

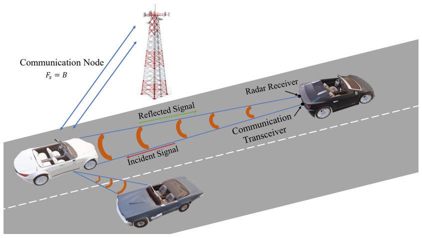

Fig. 1. In a bi-static radar scenario, an OFDM transmitter sends a signal for communication purposes. The reflections of that signal are then used by separated sensors (sub-Nyquist receivers) distributed around the transmitting vehicle to obtain radar information.

II. System Model

Consider a bi-static radar deployed for autonomous vehicles using OFDM signaling in a V2V scenario as depicted in Fig. 1. The OFDM frame consists of M symbols and N subcarriers covering a bandwidth B and separated by subcarrier spacing Δf, each symbol has a time duration $T = 1/\Delta f$ [11]. The data $d_{k,m}$ (k and m are the subcarrier and symbol indices respectively), are distributed in the time-frequency domain and modulated to time domain by performing N-point inverse fast Fourier transform (IFFT) on each symbol. After that, a cyclic prefix (CP) of duration $T_{\text{cp}} = \frac{N_{\text{cp}}}{N} T$ chosen to be greater than the maximum excess delay of the channel $\tau_{\max}$ is appended to each OFDM symbol to combat against inter-symbol interference (ISI). Then, the total OFDM symbol duration becomes $T_{\text{sym}} = T + T_{\text{cp}}$. The duration of OFDM pulse containing M symbols is assumed to be less than the coherent processing interval (CPI), that way target velocity and range are considered constant withing CPI. For transmission, the baseband signal is up-converted by carrier frequency f_c and the transmitted time-domain OFDM signal becomes

$$s_{\text{tx}}(t) = \Re\left\{\sum_{m=0}^{M-1}\sum_{k=0}^{N-1} d_{k,m}\, e^{j2\pi(f_c+k\Delta f)\ t}\, \text{rect}\left(\frac{t - mT_{\text{sym}}}{T_{\text{sym}}}\right)\right\}, \tag{1}$$

where rect(t) is the rectangular pulse function.

A. Pilot Design

The staircase pilot structure [12] is adopted in the proposed design, where each OFDM symbol contains N_p equi-spaced pilots subcarriers with spacing $S_p = \frac{N}{N_p}$. The location of the pilots in adjacent symbols is shifted with one subcarrier to form a staircase shape in each successive m OFDM symbol as illustrated in Fig. 2(a). This pilot arrangement allows pilots to cover the whole frequency band within each S_p symbol. Consequently, the data and pilots locations in the proposed OFDM frame arrangements are given as

$$d_{k,m} = \begin{cases} \text{pilot},\ k = [\eta + m]_N, \eta = 0, S_p, \ldots, (N_p - 1)S_p \\ \text{data, otherwise}. \end{cases} \tag{2}$$

whereas in [9], each two consecutive data or pilots are spaced by $\mu - 1$ empty subcarriers, thus the active subcarriers $N_{\text{a}} = \lceil \frac{N}{\mu} \rceil$, are distributed as

$$d_{k,m} = \begin{cases} \text{data},\ \ k = \mu\eta, \eta = 0, 1, \ldots, N_{\text{a}} \\ \text{zeros, otherwise}. \end{cases} \tag{3}$$

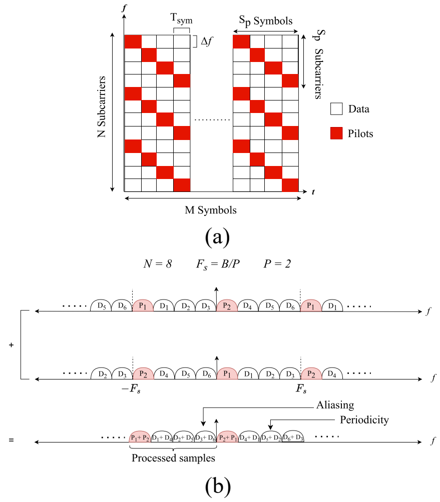

Fig. 2. Aliasing-based structure: (a) Pilots ladder-like arrangement, (b) Aliasing of subcarriers due to under-sampling where each P subcarriers spaced by $\frac{N}{P}$ are added on top of each other.

B. Channel Model

The doubly-dispersive channel is modeled such that the received signal is the sum of L reflected signals coming from sensing objects, written as

$$h(t, \tau) = \sum_{i=0}^{L-1} h_i e^{j2\pi\nu_i(t-\tau_i)}\delta(t - \tau_i), \tag{4}$$

where h_i, τ_i, and ν_i denote the attenuation coefficient, time delay and Doppler frequency shift related to the i-th path, respectively. The delay and Doppler shifts are given as

$$\tau_i = \frac{2R_i}{c} = \frac{l_i}{N\Delta f}, \quad \nu_i = \frac{2V_i f_c}{c} = \frac{k_i}{MT} \tag{5}$$

where c is the speed of light, and $l_i, k_i \in \mathbb{Q}$ denote the sampled delay and Doppler shifts corresponding to the i-th target. The distance R_i and the relative velocity V_i of the given target are extracted from the time delay and Doppler shift, respectively.

III. Pilots Aliasing-Based Radar System

The sub-Nyquist receiver, which is placed around the transmitting vehicle body, uses the reflections of the transmitted signal for sensing. The reflected signal is the output of the convolution between the transmitted signal and the channel which results in attenuated, delayed and frequency shifted replicas of the original signal plus additive white Gaussian noise (AWGN), which can be expressed as follows

$$\begin{aligned} r(t) &= s_{\text{Tx}}(t) * h(t) + n(t) \\ &= \sum_{i=0}^{L-1}\sum_{m=0}^{M-1}\sum_{k=0}^{N-1} h_i d_{k,m} e^{j2\pi(f_c+k\Delta f)(t-\tau_i)} \\ &\quad \times e^{j2\pi\nu_i(t-\tau_i)}\, \text{rect}(\beta) + n(t), \end{aligned} \tag{6}$$

where $\beta = \frac{t-\tau_i-mT_{\text{sym}}}{T_{\text{sym}}}$. Note that the noise is ignored in the following mathematical derivation for the sake of simplification. Yet, it is taken into account in the results obtained via simulation afterwards. The carrier frequency offset (CFO) is presumed to be perfectly compensated at the receiver side.

The received signal is down-converted to the baseband and the corresponding reflected signal for one target is

$$y(t)=\sum_{m=0}^{M-1}\sum_{k=0}^{N-1}\tilde{h}_i\, d_{k,m}\, e^{j2\pi k\Delta f(t-\tau_i)}\, e^{j2\pi\nu_i t}\,\mathrm{rect}(\beta), \quad (7)$$

where $\tilde{h}_i = h_i e^{-j2\pi\nu_i\tau_i} e^{-j2\pi f_c\tau_i}$. Rather than sampling the signal using the Nyquist rate (i.e., $F_s = N\Delta f$) as in conventional OFDM, in the proposed design, the received signal is under-sampled by a factor *P*. To ensure that the aliased pilots are free of data subcarriers interference the under-sampling factor *P* must be an integer multiple of S_p, which translate to the following constraints

$$P \le N_p, \quad [N_p]_P = 0. \quad (8)$$

The selection of the under-sampling ratio is therefore flexible, provided that it complies with the constraints set in (8). In contrast to [9], where modifying *P* necessitates the assignment of new values for μ at the transmitter, i.e., the pair (μ, P) is distinct and is unchangeable. The sampling rate becomes $F_s = \frac{N\Delta f}{P}$. After sampling and removing the CP, the signal is given by the formula

$$\begin{aligned} y(n) &= y(t)|_{t=\frac{nP}{N\Delta f}} = \sum_{m=0}^{M-1}\sum_{k=0}^{\frac{N}{P}-1}\sum_{p=0}^{P-1}\tilde{h}_i\, d_{k+\frac{p}{P}N,m,i}\, e^{j2\pi\frac{k(n-l_i/P)}{N/P}} \\ &\quad\times e^{j2\pi\frac{p(Pn-l_i)}{P}}\, e^{j2\pi\frac{k_iPn}{MN}}\,\mathrm{rect}\left(\frac{Pn-l_i-mN}{N}\right) \\ &= \sum_{m=0}^{M-1}\sum_{k=0}^{\frac{N}{P}-1}\tilde{h}_i\,\tilde{d}_{k,m,i}\, e^{j2\pi\frac{k\left(n-\frac{l_i}{P}\right)}{N/P}}\, e^{j2\pi\frac{k_iPn}{MN}}\,\mathrm{rect}\left(\frac{Pn-l_i-mN}{N}\right) \end{aligned} \quad (9)$$

where $\tilde{d}_{k,m,i} = \sum_{p=0}^{P-1} d_{k+\frac{p}{P}N,m}\, e^{-j2\pi\frac{pl_i}{P}}$. The under-sampled discrete time signal results in an aliased samples where each group *P* of subcarriers separated by $\frac{N}{P}$ are superimposed on top of each other as depicted in Fig. 2(b). For the aliased pilots, if the delays shifts which can be written as $l_i = \alpha_i + \beta_i P$ satisfy $[l_i]_P = \alpha_i$ where both α_i, β_i are integers, the summation $\sum_{p=0}^{P-1} e^{-j2\pi\frac{pl_i}{P}} = 0$. Hence, the channel information will be lost and the range detection will be compromised. However, since realistic delays shifts l_i's have fractional values, we assume that the aliased pilot entries $\tilde{d}_{k,m,i} \neq 0$.

To convert back the data to the time-frequency domain, we set $n = n' + m\frac{N}{P}$ with $n \in \{0, 1, \ldots, M\frac{N}{P}\}$, and then, reshape the received signal *y*(*n*) into $\mathbf{Y} \in \mathbb{C}^{\frac{N}{P}\times M}$, which is given by

$$Y_{n',m} = \tilde{h}_i e^{j2\pi\frac{k_im}{M}}\sum_{k=0}^{\frac{N}{P}-1}\tilde{d}_{k,m,i}\, e^{j2\pi\frac{k(n'-l_i/P)}{N/P}}\, e^{j2\pi\frac{k_iPn'}{MN}}. \quad (10)$$

Note that due to the rectangular pulse shaping in (9), each column of $\mathbf{Y}$ representing one OFDM symbol can be treated independently. Therefore, the fast Fourier transform (FFT) of $\mathbf{Y} \in \mathbb{C}^{\frac{N}{P}\times M}$ indicated as $\mathbf{Y}_{\mathrm{FFT}}$ is computed as follows

$$\begin{aligned} Y_{\mathrm{FFT}}(k', m) &= \sum_{i=0}^{L-1} Y_{\mathrm{FFT},i}(k', m) = \mathrm{FFT}\{Y(n', m)\} \\ &= \tilde{h}_i e^{j2\pi\frac{k_im}{M}}\sum_{k=0}^{\frac{N}{P}-1}\tilde{d}_{k,m,i}\, e^{-j2\pi\frac{kl_i}{N}}\sum_{n'=0}^{\frac{N}{P}-1} e^{j2\pi\frac{n'\left(k-k'+\frac{k_i}{MP}\right)}{N/P}}. \end{aligned} \quad (11)$$

Since $\sum_{m'=0}^{M-1} e^{j\frac{2\pi}{M}(l-l')m'} = \frac{e^{j2\pi(l-l')}-1}{e^{j\frac{2\pi}{M}(l-l')}-1}$, we can write (11) as

$$\begin{aligned} Y_{\mathrm{FFT}}(k', m) &= \tilde{h}_i e^{j2\pi\frac{k_im}{M}}\sum_{k=0}^{\frac{N}{P}-1}\tilde{d}_{k,m,i}\, e^{-j2\pi\frac{kl_i}{N}}\,\frac{e^{j2\pi\left(k-k'+\frac{k_i}{MP}\right)}-1}{e^{j\frac{2\pi}{N/P}\left(k-k'+\frac{k_i}{MP}\right)}-1}. \end{aligned} \quad (12)$$

where $\kappa_i = \frac{k_i}{MP}$ denotes the fractional Doppler shift. For $MP \gg k_i$ we can assume that $\frac{k_i}{MP} \approx 0$, then (12) becomes

$$\begin{aligned} Y_{\mathrm{FFT}}(k', m) &\approx \tilde{h}_i e^{j2\pi\frac{k_im}{M}}\sum_{k=0}^{\frac{N}{P}-1}\tilde{d}_{k,m,i}\, e^{-j2\pi\frac{kl_i}{N}}\,\delta(k-k') \\ &\approx \tilde{h}_i\tilde{d}_{k',m,i}\, e^{j2\pi\frac{k_im}{M}}\, e^{-j2\pi\frac{k'l_i/P}{N/P}}. \end{aligned} \quad (13)$$

Note that the fractional Doppler shift causes the sampling point to deviate by κ_i from the exact sampling position. This leads to loss of orthogonality between the OFDM subcarriers. Nevertheless, choosing a wide Δf results in negligible effect of that shift such that $\frac{\Delta f}{\kappa_i} \gg \epsilon$, with ϵ being a very small number. Considering that the pilots have the same complex value $p_{k+\frac{p}{P}N,m} = d_{k+\frac{p}{P}N,m} = p_{k,m}$ with $k = [\eta + m]_N, \eta = 0, S_p, \ldots, (N_p-1)S_p$, The sum of the aliased pilots in the indices (*k*, *m*) can be written as:

$$\sum_{p=0}^{P-1} p_{k+\frac{p}{P}N,m} = Pp_{k,m}, \quad \text{for } k = [\eta + m]_N. \quad (14)$$

Then, dividing by the sum of *P* pilot value $p_{k,m}$ leads to

$$D_{\mathrm{radar}}(k', m) = \frac{Y_{\mathrm{FFT}}(k', m)}{\sum_{p=0}^{P-1} p_{k+\frac{p}{P}N,m}} = \bar{h}_i e^{j2\pi\frac{k_im}{M}}\, e^{-j2\pi\frac{k'l_i/P}{N/P}} \quad (15)$$

with $\bar{h}_i$ containing different amplitude attenuation. Since $N > P$, we can approximate $\frac{k_il_i}{MN} \approx 0$. Then $\bar{h}_i$ can be written as

$$\bar{h}_i \approx h_i e^{-j2\pi\frac{f_cl_i}{N\Delta f}}\,\frac{\overbrace{\tilde{d}_{k,m,i}}^{\text{Aliased subcarriers}}}{\sum_{p=0}^{P-1} p_{k+\frac{p}{P}N,m}} \quad (16)$$

In order to obtain the range and velocity of the targets, 2-dimensional FFT operations described in [13] are applied. Thereby, for range detection an $\frac{N}{P}$-point IDFT along subcarriers is performed. Likewise, for velocity an *M*-point DFT operation along symbols is applied over the matrix $\mathbf{D}_{\mathrm{radar}}$

$$D_{\mathrm{radar}}(r, v) = \sum_{m=0}^{M-1}\sum_{k'=0}^{\frac{N}{P}-1} D_{\mathrm{radar}}(k', m)\; e^{j2\pi\frac{rk'}{N/P}}\, e^{-j2\pi\frac{vm}{M}}. \quad (17)$$

Peaks relative to the estimated ranges and relative velocities of targets will be triggered at the rows and columns of the matrix $\mathbf{D}_{\mathrm{radar}}$ for the positions and Dopplers of the targets respectively

$$r = l_i = \frac{2R_iN\Delta f}{cP}, \qquad v = k_i = \frac{2V_iMTf_c}{c}. \quad (18)$$

IV. Performance Evaluation

The parameters which are critical in the assessment of the radar performance are range and velocity resolution $(\Delta r, \Delta v)$,

TABLE I
COMPUTATIONAL COMPLEXITY

	Complexity
Standard OFDM Radar	$\mathcal{O}\left(2MN\log_2(N)\right) + \mathcal{O}(NM\log_2(M))$
Proposed Pilot Radar	$\mathcal{O}\left(2M\frac{N}{P}\log_2(\frac{N}{P})\right) + \mathcal{O}(\frac{N}{P}M\log_2(M))$

and maximum unambiguous range and velocity $(r_{\max}, v_{\max})$. As stated in [13] for OFDM, these parameters are given by

$$\Delta r = \frac{c}{2B}, \quad \Delta v = \frac{c}{2f_c M T_{\text{sym}}}. \tag{19}$$

$$r_{\max} = \frac{c}{2B}N, \quad v_{\max} = \pm\frac{c}{4f_c T_{\text{sym}}}. \tag{20}$$

A. Range and Velocity Resolution

For the pilot-aliasing (PA) processing, the whole bandwidth is used for transmission, hence the resulting range resolution Δr is similar to a standard OFDM radar, while using lower sampling rates. As such, in [9] a fraction of the bandwidth is left unused due to empty subcarriers at the edge, which reduces range resolution by $\Delta r_{diff} = \Delta r|\frac{1-\mu}{N-(\mu-1)}|$. Moreover, the proposed radar processing keeps the number of symbols unaltered, therefore the velocity resolution Δv is similar to conventional OFDM regardless of sampling rate.

B. Unambiguous Range and Velocity

Due to under-sampling, the length of each symbol will be cut to $\frac{N}{P}$. Therefore, the maximum unambiguous range is limited to

$$r_{\max} = \Delta r\frac{N}{P}. \tag{21}$$

In contrast, the maximum unambiguous velocity $v_{\max}$ remains unaffected by under-sampling because it does not impact the symbol duration T_{sym}. As opposed to SC-OFDM, each symbol is divided into M_{sub} sub-symbols, extending the symbol duration and resulting in a M_{sub} factor reduction in $v_{\max}$.

C. Computational Complexity

For radar, the ADC sampling rate will be reduced by a factor of P. Low sampling frequency reduces the computational complexity of the follow up radar process, where the matrix size shrinks to $M \times \frac{N}{P}$. For that, the required storage as well as computation complexity is reduced as shown in TABLE I. Additionally, the proposed scheme uses only the pilot value to obtain the RDM, unlike other techniques which necessitate the knowledge of the whole transmitted frame.

D. Communication Operation

The communication nodes do not under-sample the signal, thus the proposed scheme does not differ from usual OFDM's equalization, channel estimation and demodulation. As a result, similar performance in terms of bit error rate (BER), peak to average power ratio (PAPR) and spectral efficiency (SE) is obtained. The latter is given by [14]

$$SE = \log_2(1+\gamma)\big(N - N_p\big)/\big(N + N_{cp}\big). \tag{22}$$

with γ indicating the SNR. On the other hand, SA-OFDM and SC-OFDM shrink each symbol size to $N_{\text{SA}} = \frac{N}{\mu}$ and $N_{\text{SC}} = \frac{N}{M_{\text{sub}}}$, respectively, with μ representing the empty subcarriers. That reduction minimizes the transmitted data subcarriers for communication and thus lessens SE compared to OFDM.

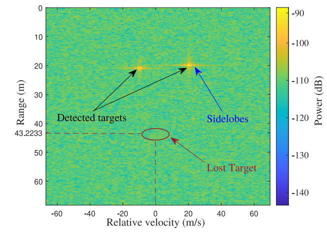

Fig. 3. Range-Doppler map for three targets using the proposed Pilot-based OFDM radar with pilot ratio $S_p = P = 4$.

TABLE II
SIMULATION PARAMETERS

Paramter	Symbol	Value		
Subcarriers	N	1024		
Symbols	M	512		
Carrier frequency (GHz)	f_c	77		
Bandwidth (MHz)	B	508		
Range $r(m)$	R_i	20	21	43.2233
Relative velocity $v(m)$	V_i	20	-10	0

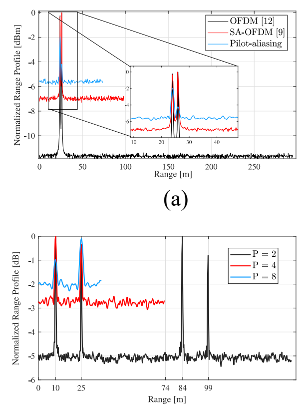

(a)

(b)

Fig. 4. Range profile comparison for: (a) The proposed OFDM Pilot-based radar versus conventional OFDM [13] and SA-OFDM [9] with $\kappa = 2$, $\mu = 3$ at $\gamma = 20$ dB, (b) Different under-sampling factors with $S_p = 4$ at $\gamma = 15$dB.

V. SIMULATION RESULTS

In this section the performance of the proposed OFDM-based radar is compared to the existing methods using the simulation parameters provided in TABLE II. The simulation considers doubly dispersive channel with zero-mean additive white Gaussian noise (AWGN) having variance σ^2.

The range-Doppler plot of the targets illustrated in Fig. 3 shows that the proposed PA radar processing can detect multiple targets correctly without abandoning the resolution as suggested in (19). However, when the delay shifts l_i's satisfy $[l_i]_P = \alpha_i$, the pilot summation $\tilde{d}_{k,m,i} = 0$, and hence the target cannot be detected as in case of $l_i = 150$ (corresponding to $r = 43.2233$) illustrated in Fig. 3. Additionally, sidelobes rise around the targets' real positions due to the aliased data-subcarriers in (16) and when α_i is non-zero fractional value, where the accuracy can be degraded by $\frac{1-e^{-j2\pi\alpha_i}}{1-e^{-j2\pi\frac{\alpha_i}{P}}}$, which can neglected and approximated to one for small α_i. Additionally, under-sampling reduces the processing gain by $10\log_{10}(P)$ dB which translates to a low target's SNR on RDM. Nevertheless, adjusting the pilot power will compensate for the SNR loss.

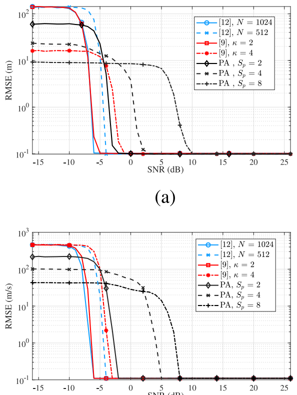

(a)

(b)

Fig. 5. RMSE of the estimated: range (a), velocity (b) versus SNR with different under-sampling factors *P* for three targets.

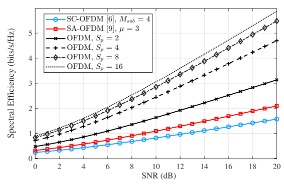

Fig. 6. Spectral efficiency comparison.

Figure 4(a) shows that the pilot-aliasing method preserves Δr when compared to SA-OFDM and OFDM, with difference in the power related to reduction in subcarriers. Figure 4(b) also shows that as P increases, $r_{\max}$ is reduced according to (21) without affecting the resolution of the radar detection. Besides, choosing P less than S_p repeats range profile every $r_{\max}$ (calculated with reference to S_p) since the same information is taken from the sampled subcarriers which have periodic behaviour as shown in Fig. 2 (b). Therefore, sufficient information is obtained if we under-sample by $P = S_p$. Moreover, $P > S_p$ enhances only the SNR in the RDM (more samples), without extending either Δr or $r_{\max}$.

Figure 5(a) illustrates a comparison between the proposed method and other techniques in terms of root mean square error (RMSE) of the estimated and exact target positions at various SNR values. For low SNR, the error probability is high, but it converges to a constant value due to the predefined bandwidth after a certain SNR threshold, while the target resolvability remains unaltered. Retaining the same RMSE while minimizing the sampling rate (high values of P) necessitates greater SNR. Furthermore, compared to SA-OFDM, the proposed method requires 4 dB more SNR to achieve comparable RMSE (for P = 4) due to the loss of SNR caused by aliased data-subcarriers. Similarly, in Fig. 5 (b), the velocity RMSE of various algorithms converged to the same value after an SNR threshold because of a fixed symbol duration. Additionally, the proposed method maintains accurate velocity estimation capabilities in comparison to other techniques, whereas increasing P necessitates a high SNR to achieve the same RMSE value in order to compensate for the loss of SNR caused by aliasing.

For communication, the SE of different methods is compared with the same modulation order and transmission bandwidth, no guard between the subcarriers is left. As illustrated in Fig. 6, the proposed approach does not compromise the SE for communication, in contrast to SA-OFDM and SC-OFDM which significantly degrade the communication throughput.

VI. Conclusion

This letter proposes a peculiar technique for OFDM-based radar to achieve high-range resolution at a cost-effective ADC sampling frequency. The pilots are arranged in a ladder-like pattern according to a predetermined ratio S_p, which defines the under-sampling ratio. Simulation results indicate that radar performance in terms of HRR sensing is roughly comparable for various pilot ratios, with a negligible degradation when employing higher P values due to low SNR resulting from aliased data subcarriers and few sampled subcarriers. The proposed method permits sensors to derive high-resolution information about a target using only the pilot's value and a minimal receiver complexity.

References

[1] Z. Feng, Z. Fang, Z. Wei, X. Chen, Z. Quan, and D. Ji, "Joint radar and communication: A survey," *China Commun.*, vol. 17, no. 1, pp. 1–27, Jan. 2020.

[2] T. Zugno, M. Drago, M. Giordani, M. Polese, and M. Zorzi, "Toward standardization of millimeter-wave vehicle-to-vehicle networks: Open challenges and performance evaluation," *IEEE Commun. Mag.*, vol. 58, no. 9, pp. 79–85, Sep. 2020.

[3] M. S. J. Solaija, S. E. Zegrar, and H. Arslan, "Orthogonal frequency division multiplexing: The way forward for 6G physical layer design?" *IEEE Veh. Technol. Mag.*, early access, Jan. 8, 2024, doi: 10.1109/MVT.2023.3344432.

[4] J. A. Zhang et al., "Enabling joint communication and radar sensing in mobile networks—A survey," *IEEE Commun. Surveys Tuts.*, vol. 24, no. 1, pp. 306–345, 1st Quart., 2022.

[5] G. Hakobyan and B. Yang, "High-performance automotive radar: A review of signal processing algorithms and modulation schemes," *IEEE Signal Process. Mag.*, vol. 36, no. 5, pp. 32–44, Sep. 2019.

[6] B. Schweizer, C. Knill, D. Schindler, and C. Waldschmidt, "Stepped-carrier OFDM-radar processing scheme to retrieve high-resolution range-velocity profile at low sampling rate," *IEEE Trans. Microw. Theory Techn.*, vol. 66, no. 3, pp. 1610–1618, Mar. 2018.

[7] C. Knill, B. Schweizer, S. Sparrer, F. Roos, R. F. H. Fischer, and C. Waldschmidt, "High range and doppler resolution by application of compressed sensing using low baseband bandwidth OFDM radar," *IEEE Trans. Microw. Theory Techn.*, vol. 66, no. 7, pp. 3535–3546, Jul. 2018.

[8] B. Nuss, J. Mayer, S. Marahrens, and T. Zwick, "Frequency comb OFDM radar system with high range resolution and low sampling rate," *IEEE Trans. Microw. Theory Techn.*, vol. 68, no. 9, pp. 3861–3871, Sep. 2020.

[9] O. Lang, R. Feger, C. Hofbauer, and M. Huemer, "OFDM radar with subcarrier aliasing—Reducing the ADC sampling frequency without losing range resolution," *IEEE Trans. Veh. Technol.*, vol. 71, no. 10, pp. 10241–10253, Oct. 2022.

[10] M. Hua, Q. Wu, W. Chen, A. Jamalipour, and O. A. Dobre, "Integrated sensing and communication: Joint pilot and transmission design," 2022, *arXiv:2211.12891*.

[11] C. Sturm and W. Wiesbeck, "Waveform design and signal processing aspects for fusion of wireless communications and radar sensing," *Proc. IEEE*, vol. 99, no. 7, pp. 1236–1259, Jul. 2011.

[12] D. V. Adakane and K. Vasudevan, "An efficient pilot pattern design for channel estimation in OFDM systems," in *Proc. IEEE Int. Conf. Signal Process. Comput. Control (ISPCC)*, 2013, pp. 1–5.

[13] C. Sturm, E. Pancera, T. Zwick, and W. Wiesbeck, "A novel approach to OFDM radar processing," in *Proc. IEEE Radar Conf.*, 2009, pp. 1–4.

[14] L. Dai, Z. Wang, and Z. Yang, "Time-frequency training OFDM with high spectral efficiency and reliable performance in high speed environments," *IEEE J. Sel. Areas Commun.*, vol. 30, no. 4, pp. 695–707, May 2012.